

Broken ergodicity of right triangular billiard systems

Junxiang Huang* and Hong Zhao†

*Department of Physics and Institute of Theoretical Physics and Astrophysics,
Xiamen University, Xiamen 361005, Fujian, China*

(Dated: June 15, 2019)

A right triangular billiard system is equivalent to the system of two colliding particles confined in a one-dimensional box. In spite of their seeming simplicity, no definite conclusion has been drawn so far concerning their ergodic properties. To answer this question, we transform the dynamics of the right triangular billiard system to a piecewise map and analytically prove the broken ergodicity. The mechanism leading to the broken ergodicity is discussed, and some numerical evidence corroborating our conclusion is provided.

PACS numbers: 05.45.a, 05.90.+m

I. INTRODUCTION

The conventional hypothesis used in statistical mechanics is that the time average of a system is equal to its ensemble average in the limit of long measurement time t because of its ergodicity. However, if a system has a lot of metastable states, its phase trajectories may be trapped in some subset of its total phase space for long times. Consequently, the real behaviors often differ from the predictions based on the usual Gibbs formalism. Though abundant related research results have been obtained, studies on the dynamical and thermal properties of these nonergodic systems still largely rely on intuition and simple pictures of the phase spaces due to the lack of a real theory [1], which stimulates interest in the ergodic properties of variant disordered systems such as glass systems [2, 3] and random walk models [4].

Another class of model systems whose ergodic properties have been studied for a long time are polygonal billiards [5]. A remarkable theorem of Ref. [6] shows that the one-parameter family of directional flows f_θ^t are uniquely ergodic for Lebesgue almost all $\theta \in [0, 2\pi)$. In particular, this theorem says that the directional billiard flow of a rational polygon, namely, all of its vertex angles are rational multiples of π , is ergodic for almost every direction. Ref. [7] lists some open problems of polygonal billiard dynamics, including how to give an explicit example of an irrational but nonergodic polygonal billiard.

As a relatively simple polygonal billiard, the right triangular billiard has been studied extensively on its ergodic properties. On one hand, it is generally acknowledged that the billiard flow in a rational right triangle, namely, the acute angles of a right triangle are rational multiples of π , is nonergodic [8]. On the other hand, we know much less about the irrational cases. It is well known that a right triangular billiard is equivalent to the system of two hard particles colliding with each other and the walls in a one-dimensional box [9]. Some researchers

have already investigated the ergodic properties of both models, but did not get a definitive conclusion: while some previous studies announced that for some special parameters the former model is ergodic [10], there is numerical evidence suggested that the latter model is not [11, 12]. However, since these two models are equivalent, their ergodic properties must be identical.

Moreover, a prevailing opinion is that nonergodic Hamiltonian systems usually display a very complicated and intricate structure of stable island in the phase space among a sea of chaotic trajectories [13]. However, the right triangular billiard does not belong to this situation. So if it is nonergodic, it may shed light to the study of finding other nonergodic mechanisms without the presence of divided phase space.

This paper provides an easier-to-manipulate method to study right triangular billiard than that previous studies used. By this method, we prove that the billiard flow is nonergodic due to localization in the velocity direction of the particle. Besides, we give an explanation to the contradiction between previous studies, and answer another open question listed in Ref. [7].

Due to singularities in the billiard flow, the phase trajectories are discontinuous. Based on our understanding of this fact, we transform the original model into a two-dimensional piecewise map in Sec. II. Then we focus on the map instead of the original model, all of whose important properties are retained in the map. Some of these properties, which are explored with the help of symbolic sequence analysis in Sec. III, play a key role in the proof of the broken ergodicity in Sec. IV. After that, the mechanism leads to ergodicity breaking will be discussed in Sec. V. We also make extended discussions in Sec. VI.

II. THE MODELS

A right triangular billiard system describes the motion of a particle reflecting from the sides elastically in a right triangle. The only control parameter of the system is the acute angle $\alpha \in (0, \pi/2)$. To describe the state of the particle at an arbitrary moment, i.e. to pin down a point in the whole phase space, we need three

*Electronic address: mockingwizard@gmail.com

†Electronic address: zhaoh@xmu.edu.cn

variables: two represent its position and one represents its velocity-direction. The speed is a constant because all collisions are elastic. However, if we focus on the instants the particle collides with the hypotenuse, the two position variables collapse to one variable x , i.e. the location where the particle collides with the hypotenuse. We fix the length of the hypotenuse to be unity and set the α vertex point to be the origin, then we have $x \in [0, 1]$. The velocity-direction variable is represented as the rebound angle $\theta \in (0, \pi)$ measured as Fig. 1 shows. In other words, we use two variables θ and x to make a Poincaré section of the phase space.

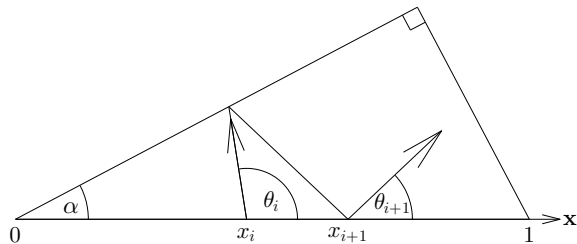


FIG. 1: A particle moves in a right triangular billiard whose hypotenuse has unit length. The collisions between the particle and the sides are all elastic. The motion in the figure from leaving x_i to colliding with the hypotenuse at x_{i+1} is denoted by a letter R , whose mapping formula for θ and x can be derived using the law of sines.

The dynamics of the original model can be reduced to a simpler form. Between two consecutive collisions with the hypotenuse, there are three possible events. If we fix the x_i value and vary θ_i from 0 to 2π , these three events will appear in the following order: (1) only one collision with the opposite side of α , (2) two collisions with both legs respectively, (3) only one collision with the adjacent side of α . Motivated on this fact, we separate the motion of the particle at every instant right after it collides with the hypotenuse, and denote the combination of a collision with the hypotenuse and the followed event by L , M , and R , respectively. In other words, every letter represents one collision with the hypotenuse plus one or two collisions with the legs. For example, as illustrated in Fig. 1, a letter R represents the motion starts from the instant right after the particle collides with the hypotenuse, through a collision with the adjacent side of α , to the next collision with the hypotenuse. Using the relation of the angles and the law of sines, we have

$$\mathbf{R} : \begin{cases} \theta_{i+1} = \theta_i - 2\alpha \\ x_{i+1} = x_i \frac{\sin \theta_i}{\sin(\theta_i - 2\alpha)} \end{cases} \quad (1)$$

In this paper we use such a bold-type letter to represent a mapping operation. To simplify the formulas, we introduce a new variable

$$\vartheta = \frac{\sin(\theta - 2\alpha)}{\sin \theta} \in (-\infty, \infty) \quad (2)$$

to replace the variable θ . Denoting a new parameter $a = 2 \cos 2\alpha \in (-2, 2)$, the conditions and formulas of forward iteration can be written as:

$$\mathbf{L} : \begin{cases} \vartheta_{i+1} = a - \frac{1}{\vartheta_i} \\ x_{i+1} = -\frac{x_i}{\vartheta_i} + \frac{1}{\vartheta_i} + 1 \end{cases} \quad (3a)$$

for $\vartheta_i < 0$, $x_i > 1 + \vartheta_i$;

$$\mathbf{M} : \begin{cases} \vartheta_{i+1} = a - \vartheta_i \\ x_{i+1} = 1 + \vartheta_i - x_i \end{cases} \quad (3b)$$

for $-1 \leq \vartheta_i \leq 1$, $\vartheta_i \leq x_i \leq 1 + \vartheta_i$;

$$\mathbf{R} : \begin{cases} \vartheta_{i+1} = a - \frac{1}{\vartheta_i} \\ x_{i+1} = \frac{x_i}{\vartheta_i} \end{cases} \quad (3c)$$

for $\vartheta_i > 0$, $x_i < \vartheta_i$.

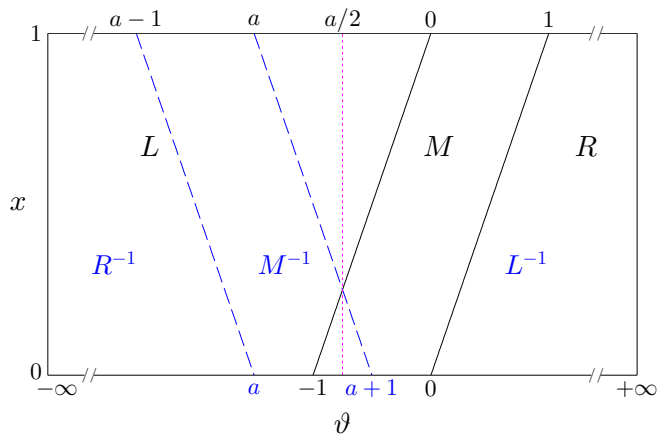


FIG. 2: (Color online) The forward iteration regions L , M , and R are partitioned by solid black lines. The backward iteration regions R^{-1} , M^{-1} , and L^{-1} are partitioned by dashed blue lines. The forward and backward iteration regions are symmetric with respect to the dotted line $\vartheta = a/2$.

This piecewise map describes the evolution rules on the Poincaré section, so it is equivalent to the dynamics of right triangular billiard. As shown in Fig. 2, in light of these equations we can partition the ϑ - x plane into three forward regions correspond to L , M , and R , respectively. A phase point is mapped to its next image according to which region it belongs to. Performing the same procedure for its images, we can obtain its infinite forward symbolic sequence made of letter L , M , and R . A typical infinite forward sequence may be written as $\bullet P_1 P_2 P_3 \dots$, where \bullet denotes the present state and P_i represents an L , M , or R [14]. The points correspond to this infinite forward sequence belong to P_1 region, then they are mapped to P_2 region following P_1 part of Eq. (3), etc.

A symmetry of the original model is in the parameter space: if we observe Fig. 1 from behind the paper, then

the parameter α becomes $\alpha' = \pi/2 - \alpha$, and $\theta' = \pi - \theta$, $x' = 1 - x$. The corresponding symmetry of the piecewise map appears as $a' = -a$, $\vartheta' = -\vartheta$, and $x' = 1 - x$. This means the system with parameter a is equivalent to that with parameter $-a$. So it is sufficient to study only cases with $a \in (-2, 0]$ (corresponding to $\alpha \in [\pi/4, \pi/2)$) or $a \in [0, 2)$ (corresponding to $\alpha \in (0, \pi/4]$).

The formulas of backward iteration can be derived from Eq. (3):

$$\mathbf{R}^{-1} : \begin{cases} \vartheta_i = \frac{1}{a - \vartheta_{i+1}} \\ x_i = \frac{x_{i+1}}{a - \vartheta_{i+1}} \end{cases} \quad (4a)$$

for $\vartheta_{i+1} < a$, $x_{i+1} < a - \vartheta_{i+1}$;

$$\mathbf{M}^{-1} : \begin{cases} \vartheta_i = a - \vartheta_{i+1} \\ x_i = 1 + a - \vartheta_{i+1} - x_{i+1} \end{cases} \quad (4b)$$

for $a - 1 \leq \vartheta_{i+1} \leq a + 1$, $a - \vartheta_{i+1} \leq x_{i+1} \leq 1 + a - x_{i+1}$;

$$\mathbf{L}^{-1} : \begin{cases} \vartheta_i = \frac{1}{a - \vartheta_{i+1}} \\ x_i = -\frac{x_{i+1}}{a - \vartheta_{i+1}} + \frac{1}{a - \vartheta_{i+1}} + 1 \end{cases} \quad (4c)$$

for $\vartheta_{i+1} > a$, $x_{i+1} > 1 + a - \vartheta_{i+1}$.

Likewise, we can partition the ϑ - x plane into three backward regions correspond to R^{-1} , M^{-1} , and L^{-1} , respectively. A typical infinite backward sequence may be written as $\cdots Q_3 Q_2 Q_1 \bullet$, where Q_i represents a R^{-1} , M^{-1} , or L^{-1} and Q_1 iteration happened most recently. Generally speaking, a phase point one-to-one corresponds to a bi-infinite sequence $\cdots Q_3 Q_2 Q_1 \bullet P_1 P_2 P_3$ (if exists). In the following, we use the word ‘‘sequence’’ while its length is finite unless otherwise indicated.

III. SEVERAL IMPORTANT PROPERTIES

Above we reduce the dynamics of the original model to a two-dimensional map on the ϑ - x plane, which is a Poincaré section of the phase space. If the original model is ergodic, the trajectories of the map must be dense on the ϑ - x plane. Otherwise, the ergodicity of the model is broken.

For the sake of convenience, if a sequence contains an even number of M , we call it an even sequence; otherwise we call it an odd sequence. Below we consider only even sequences first. Denoting by S a letter L or R , we let \tilde{n} be the difference between the total number of S in odd position (right after the $2k$ -th M , $k = 0, 1, 2, \dots$) and in even positions (right before the $2k$ -th M , $k = 0, 1, 2, \dots$). For example, $\tilde{n}(SSMSM) = 1$, and $\tilde{n}(MSSSM) = -3$. Below we will show that this difference \tilde{n} is an important property of a sequence. In Eq. (3), though which map the phase point will follow is partly depend on the x

values, the evolution formulas for ϑ do not request exact x values, so we can calculate ϑ_N according to only ϑ_0 and the sequence $P_1 \cdots P_N$. Therefore, it is convenient to use $\vartheta_N = \mathbf{P}_1 \cdots \mathbf{P}_N \vartheta_0$ to record this relation, where ϑ_N is the ϑ value of (ϑ_0, x_0) ' N_{th} image. Then we have

$$\begin{aligned} \mathbf{SMS} \vartheta &= \mathbf{M} \vartheta = a - \vartheta \\ \mathbf{MM} \vartheta &= \vartheta. \end{aligned} \quad (5)$$

Eq. (5) provides two rules, based on which we can calculate whether two sequences have identical effect on the ϑ variable. Surprisingly, we find that the effect of an even sequence on the ϑ variable depends only on its difference \tilde{n} , i.e. equals to that of sequence $S^{\tilde{n}}$. Take the sequences mentioned above for example. $\mathbf{SSMSM} \vartheta_0 = \mathbf{S} \vartheta_0$, and $\mathbf{MSSSM} \vartheta_0 = \mathbf{S}^{-3} \mathbf{S}^3 \mathbf{M} \mathbf{S}^3 \mathbf{M} \vartheta_0 = \mathbf{S}^{-3} \vartheta_0$. Therefore, the ϑ value of the image after an even sequence $P_1 \cdots P_N$ is a function of ϑ_0 and \tilde{n} , which can be denoted by

$$\Theta(\vartheta_0, \tilde{n}) = \mathbf{S}^{\tilde{n}} \vartheta_0, \quad (6)$$

On the x part, to simplify the notation, it is convenient to use $x_N = \mathbf{P}_1 \cdots \mathbf{P}_N x_0$ to record the evolution of x values following a sequence $P_1 \cdots P_N$, where x_N is the x value of (ϑ_0, x_0) ' N_{th} image. Here we omit the ϑ part of the coordinate for convenience, but this does not mean the evolution of x is independent with ϑ . Actually, when we calculate the x_{i+1} in practice, we must take ϑ_i into consideration. But since the ϑ_i can be derived from ϑ_0 and the sequence, this omission is reasonable. Using such notations, given an infinitesimal perturbation $d(x_0)$ in the x direction, we have

$$\begin{aligned} |d(\mathbf{S}x_0)| &= \left| \frac{d(x_0)}{\vartheta_0} \right| \\ |d(\mathbf{SMS}x_0)| &= |d(\mathbf{M}x_0)| = |d(x_0)|. \end{aligned} \quad (7)$$

Here we assume that an infinitesimal perturbation does not change the forward sequence. Likewise, we can use Eq. (7) to calculate the effect of an even sequence on the images with a tiny perturbation in the x direction. We find that the effect of an even sequence on the perturbation of image depends only on its difference \tilde{n} , i.e. equals to that of sequence $S^{\tilde{n}}$. For example, $|d(\mathbf{SSMSM}x_0)| = |d(\mathbf{S}x_0)|$, and $|d(\mathbf{MSSSM}x_0)| = |d(\mathbf{S}^{-3}x_0)|$. Therefore, the stretch rate in the x direction is also a function of ϑ_0 and \tilde{n} , which can be denoted by

$$\Omega(\vartheta_0, \tilde{n}) = \left| \frac{d(\mathbf{S}^{\tilde{n}}x_0)}{d(x_0)} \right|. \quad (8)$$

These two functions are the keys to proving the broken ergodicity. The next thing we need to do is to derive their expressions by introducing an intermediate variable. Define an array $\{W(\vartheta_0, \tilde{n}) \mid \tilde{n} \in \mathbb{Z}\}$ by

$$\begin{cases} W(\vartheta_0, \tilde{n} + 1) = \Theta(\vartheta_0, \tilde{n})W(\vartheta_0, \tilde{n}) \\ W(\vartheta_0, 0) = 1. \end{cases} \quad (9)$$

According to Eq. (6), we have

$$\begin{aligned}\Theta(\vartheta_0, \tilde{n}) &= \mathbf{S}\Theta(\vartheta_0, \tilde{n} - 1) \\ &= a - 1/\Theta(\vartheta_0, \tilde{n} - 1).\end{aligned}\quad (10)$$

Using it in Eq. (9), we get

$$\begin{aligned}W(\vartheta_0, \tilde{n} + 1) &= \left[a - \frac{1}{\Theta(\vartheta_0, \tilde{n} - 1)} \right] W(\vartheta_0, \tilde{n}) \\ &= aW(\vartheta_0, \tilde{n}) - W(\vartheta_0, \tilde{n} - 1).\end{aligned}\quad (11)$$

Then by the undetermined coefficient method, we obtain

$$\begin{aligned}W(\vartheta_0, \tilde{n}) &= \frac{\vartheta_0(e^{i2\tilde{n}\alpha} - e^{-i2\tilde{n}\alpha}) - (e^{i2(\tilde{n}-1)\alpha} - e^{-i2(\tilde{n}-1)\alpha})}{e^{i2\alpha} - e^{-i2\alpha}} \\ &= \frac{\vartheta_0 \sin(2\tilde{n}\alpha) - \sin(2(\tilde{n} - 1)\alpha)}{\sin(2\alpha)} \\ &= \frac{\sqrt{\vartheta_0^2 - a\vartheta_0 + 1}}{\sin(2\alpha)} \sin(2\tilde{n}\alpha + \psi),\end{aligned}\quad (12)$$

where

$$\psi = \arcsin\left(\frac{\sin(2\alpha)}{\sqrt{\vartheta_0^2 - a\vartheta_0 + 1}}\right).\quad (13)$$

Based on the expression of $W(\vartheta_0, \tilde{n})$, it follows that if a phase point (ϑ_0, x_0) follows an even sequence $P_1 \cdots P_N$ with \tilde{n} , the ϑ value of the N_{th} image is

$$\begin{aligned}\Theta(\vartheta_0, \tilde{n}) &= \frac{\sin(2(\tilde{n} + 1)\alpha + \psi)}{\sin(2\tilde{n}\alpha + \psi)} \\ &= \cot(2\tilde{n}\alpha + \psi) \sin(2\alpha) + \cos(2\alpha),\end{aligned}\quad (14)$$

and the stretch rate in the x direction is

$$\begin{aligned}\Omega(\vartheta_0, \tilde{n}) &= \frac{\Omega(\vartheta_0, \tilde{n} - 1)}{|\Theta(\vartheta_0, \tilde{n} - 1)|} = \left| \frac{W(\vartheta_0, \tilde{n} - 1)}{W(\vartheta_0, \tilde{n})} \right| \Omega(\vartheta_0, \tilde{n} - 1) \\ &= \left| \frac{W(\vartheta_0, \tilde{n} - 1)}{W(\vartheta_0, \tilde{n})} \cdots \frac{W(\vartheta_0, 0)}{W(\vartheta_0, 1)} \right| \Omega(\vartheta_0, 0) \\ &= \frac{1}{|W(\vartheta_0, \tilde{n})|} = \frac{\sin(2\alpha)}{\sqrt{\vartheta_0^2 - a\vartheta_0 + 1}} \frac{1}{|\sin(2\tilde{n}\alpha + \psi)|}.\end{aligned}\quad (15)$$

Similar calculation applied on cases of odd sequences yields that if a phase point (ϑ_0, x_0) follows a sequence $P_1 \cdots P_N$ with \tilde{n} , the ϑ value of the N_{th} image is

$$\vartheta_N = \begin{cases} \cot(2\tilde{n}\alpha + \psi) \sin(2\alpha) + \cos(2\alpha), & \text{if } P_1 \cdots P_N \text{ is an even sequence;} \\ a - [\cot(2\tilde{n}\alpha + \psi) \sin(2\alpha) + \cos(2\alpha)], & \text{if } P_1 \cdots P_N \text{ is an odd sequence;} \end{cases}\quad (16)$$

and the stretch rate in the x direction is

$$\Omega(\vartheta_0, \tilde{n}) = \frac{\sin(2\alpha)}{\sqrt{\vartheta_0^2 - a\vartheta_0 + 1}} \frac{1}{|\sin(2\tilde{n}\alpha + \psi)|}.\quad (17)$$

IV. THE BROKEN ERGODICITY

We will prove the broken ergodicity of all right triangular billiards in this section. To begin with, let us see how to connect the ergodic property with symbolic sequences. On one hand, cases of rational π/α are easy to deal with. Eq. (16) indicates that with fixed ϑ_0 , ϑ_N is either $\Theta(\vartheta_0, \tilde{n})$ or $a - \Theta(\vartheta_0, \tilde{n})$. Since $\Theta(\vartheta_0, \tilde{n})$ is a periodic function with period $\pi/(2\alpha)$ on \tilde{n} , if π/α is rational, the images of all points on line $\vartheta = \vartheta_0$ can take only a finite number of ϑ values, which results in broken ergodicity. An equivalent result was suggested by Artuso et al. in Ref. [8].

On the other hand, to solve the problem of irrational cases, which is the main purpose of this paper, some more complicated analysis is needed. Arbitrarily choose an initial point (ϑ_0, x_0) with irrational π/α , we are able to calculate how many different ϑ values its first N images can take according to the first N letters of its forward sequence. There exists an upper limit $2(\tilde{n}_{\text{max}} - \tilde{n}_{\text{min}} + 1)$ for this number, where \tilde{n}_{max} (respectively \tilde{n}_{min}) is the maximum (respectively the minimum) of \tilde{n} the sequence ever took. A trajectory which is dense in the phase space must take infinite number of ϑ values.

Therefore, the broken ergodicity of the model will be proved if we show that the upper limit of almost every initial point remains finite while $N \rightarrow +\infty$. Motivated by this purpose, let us first define $E(\vartheta_0, \tilde{n})$ as the set of initial points on line $\vartheta = \vartheta_0$ that will be mapped to $\vartheta = \Theta(\vartheta_0, \tilde{n})$ or $\vartheta = a - \Theta(\vartheta_0, \tilde{n})$ before return to $\vartheta = \vartheta_0$, as illustrated in Fig. 3. According to this definition, the set E has two properties: (1) if a point on line $\vartheta = \vartheta_0$ is mapped to line $\vartheta = \Theta(\vartheta_0, \tilde{n})$ or $\vartheta = a - \Theta(\vartheta_0, \tilde{n})$, it must be a pre-image or an element of $E(\vartheta_0, \tilde{n})$; (2) $E(\vartheta_0, \tilde{n})$ is a subset of $E(\vartheta_0, \tilde{n}')$ for $\tilde{n}/\tilde{n}' > 1$ since \tilde{n} is further from 0 than \tilde{n}' is.

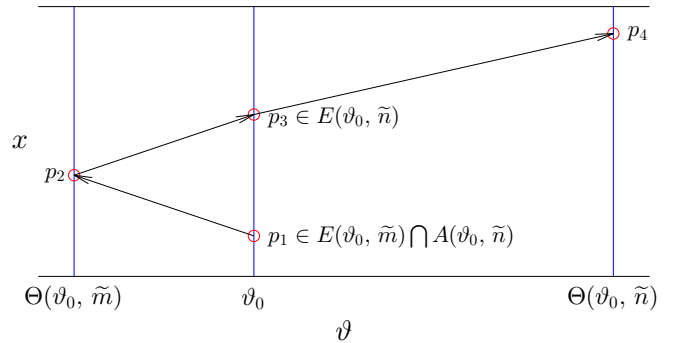


FIG. 3: Points p_i ($i = 1, 2, 3, 4$) belong to the same trajectory, but they may be not adjacent. Both p_1 and p_3 are on line $\vartheta = \vartheta_0$. According to our definitions, since p_1 is mapped to $\Theta(\vartheta_0, \tilde{m})$ before ever returning to ϑ_0 , it belongs to $E(\vartheta_0, \tilde{m})$. Similarly, p_3 belongs to $E(\vartheta_0, \tilde{n})$. On the contrary, p_1 is mapped back to line $\vartheta = \vartheta_0$ before it is ever mapped to line $\vartheta = \Theta(\vartheta_0, \tilde{n})$ or $\vartheta = a - \Theta(\vartheta_0, \tilde{n})$, so it belongs to $A(\vartheta_0, \tilde{n})$ but not to $E(\vartheta_0, \tilde{n})$.

The next thing to do is to show that $E(\vartheta_0, \pm\infty)$ has (one-dimensional) measure zero for arbitrary ϑ_0 . Let $\varepsilon > 0$ be given. We can find a large K such that there exist $-K < \tilde{n}_1 < 0 < \tilde{n}_2 < K$ and $\max(|W(\vartheta_0, \tilde{n}_1)|, |W(\vartheta_0, \tilde{n}_2)|) < \varepsilon/2$. Denoting by μ the (one-dimensional) measure of $E(\vartheta_0, \tilde{n}_2)$, because every point in $E(\vartheta_0, \tilde{n}_2)$ has one or two “first-time-arrival” images on lines $\vartheta = \Theta(\vartheta_0, \tilde{n}_2)$ and $\vartheta = a - \Theta(\vartheta_0, \tilde{n}_2)$, the set of all these images has measure μ' such that $\mu/|W(\vartheta_0, \tilde{n}_2)| \leq \mu' \leq 2\mu/|W(\vartheta_0, \tilde{n}_2)|$ due to the stretch rate $1/|W(\vartheta_0, \tilde{n}_2)|$.

If $\mu \geq \varepsilon$, then μ' is bigger than 2. Since the map is reversible, these “first-time-arrival” images of $E(\vartheta_0, \tilde{n}_2)$ cannot overlap. This contradicts the fact that the total measure of line segments $\vartheta = \Theta(\vartheta_0, \tilde{n}_2)$ and $\vartheta = \Theta(\vartheta_0, \tilde{n}_2)$ is just 2. Therefore, the measure of $E(\vartheta_0, \tilde{n}_2)$ must be smaller than ε . Consequently, due to the property (2) of $E(\vartheta_0, \tilde{n}_2)$, the measure of $E(\vartheta_0, K)$ is smaller than the measure of $E(\vartheta_0, \tilde{n}_2)$, and thus is smaller than ε . Likewise, the measure of $E(\vartheta_0, -K)$ is also smaller than ε . Since ε is arbitrary, it implies that $E(\vartheta_0, \pm\infty)$ has measure zero.

Then we try to weaken the conditions. We define $A(\vartheta_0, \tilde{n})$ as the set of points on line $\vartheta = \vartheta_0$ that will be mapped to $\vartheta = \Theta(\vartheta_0, \tilde{n})$ or $\vartheta = a - \Theta(\vartheta_0, \tilde{n})$. According to the property (1) of $E(\vartheta_0, \tilde{n})$, any point belongs to $A(\vartheta_0, \tilde{n})$ is either a pre-image or an element of $E(\vartheta_0, \tilde{n})$. Therefore, $A(\vartheta_0, \pm\infty)$ has measure zero as well, because a point has only a countable number of pre-images. We have thus proved that almost every point with fixed initial ϑ_0 can take only a finite number of different ϑ values no matter how many iterations have been taken.

It is worth mentioning that the ratio between the measure of $A(\vartheta_0, \tilde{n})$ and that of its “first-time-arrival” images on lines $\vartheta = \Theta(\vartheta_0, \tilde{n})$ and $\vartheta = a - \Theta(\vartheta_0, \tilde{n})$ may be smaller than 1/2 since a single “first-time-arrival” image could correspond to many points in $A(\vartheta_0, \tilde{n})$. This is why we use the measure of $E(\vartheta_0, \tilde{n})$ as an immediate variable.

Finally, we can construct a subset of the phase plane to prove the broken ergodicity. Choose a small ξ , then for arbitrary $\vartheta_0 \in [(a - \xi)/2, (a + \xi)/2]$, we exclude the exceptional points which belong to a set with (one-dimensional) measure zero. After that, the remain subset Λ still has a positive (two-dimensional) measure, and every point in Λ can be mapped to only a finite number of different ϑ values. Decrease ξ such that $\xi/\rho \leq 1$, where ρ is the minimum of $\{\cos^2(2\tilde{n}\alpha) \mid \tilde{n} \in [K_-, K_+]\}$. Obviously, no matter how many forward iterations have been taken, there is some ϑ values no images of Λ can take. In other words, $\bigcup_{N=1}^{+\infty} \mathbf{T}^N \Lambda$, the set of the images of Λ , is only a proper subset of the phase plane, where \mathbf{T} represents a forward iteration. Let Λ' be the symmetric set of Λ with respect to line $\vartheta = a/2$, then the result can be written as $\bigcup_{N=1}^{+\infty} \mathbf{T}^{-1N} \Lambda'$ is only a proper subset of the phase plane (see Sec. V). Hence the broken ergodicity is proved.

One might argue that $\bigcup_{N=1}^{+\infty} \mathbf{T}^N \Lambda$ is only a proper sub-

set of the phase plane may result from the infinity of the ϑ - x plane. To resolve this doubt, we rewrite the result gotten before the final step as “almost every point with fixed initial θ_0 can take only a finite number of different θ values no matter how many iterations have been taken”, then perform the final step in θ - x plane, where iterations keep the length in the θ direction and the whole phase plane is finite. The same conclusion can be obtained.

V. THE MECHANISM

The interdependence between the ϑ of the image and the stretch rate in the x direction restricts the number of different ϑ values a trajectory can take, thus the system is nonergodic. Next we explain the mechanism of the ergodicity breaking. If one observes a symbolic sequence of an arbitrary trajectory, he could find many sequence fragments whose $\tilde{n} = 0$. According to Eq. (5), the ϑ value of the phase point before such a fragment and that after the same fragment are equal or symmetric with the respect to line $\vartheta = a/2$. In other words, these “inefficient” sequence fragments make the images meander within several ϑ values for long times. The lengths of these sequence fragments we ever observed vary from only several letters to 10^5 or even more letters, implying that such phenomena appear in various time scales.

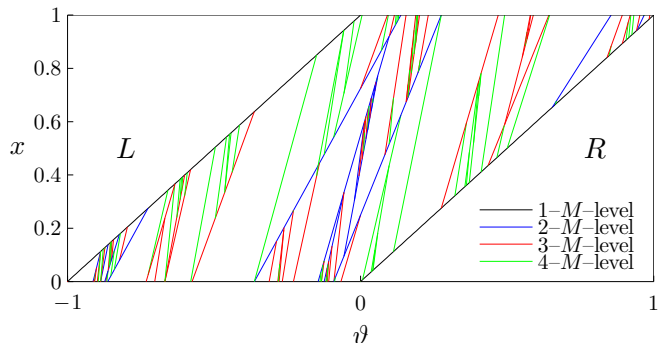


FIG. 4: (Color online) The partition lines in the M region up to 4- M -level, i.e., points belong to the same small region share a common string which includes four M letters. High-level partition lines are steeper than low-level partition lines.

Several special properties are responsible for these “inefficient” sequence fragments. One of these properties is about the scopes of the partition lines in the phase plane. The phase plane can be partitioned into different regions. Points belong to the same region share a common string at the beginning of their infinite sequences. Of course, while we increase the length of the common string, part of these points will not satisfy this condition, and a big region can be partitioned into several smaller regions. Partition lines are the boundaries of the regions, so they can be classified to different levels. In practice, we can obtain these partition lines by backward iterating the LM and MR partition lines, which are two straight-line segments.

Since \mathbf{R}^{-1} , \mathbf{M}^{-1} and \mathbf{L}^{-1} all map a line segment to another line segment, the partition lines in the phase plane are all straight-line segments. Fig. 4 shows some low-level partition lines in the M region. One can see that as the levels of partition lines increase, the scopes of the partition lines increase either. This feature results in that the phase plane is partitioned into many slender almost-vertical regions, and thus increases the average length of common strings two nearby points with the same ϑ value share. In other words, when a point is mapped to the same ϑ and changes a bit on x , it is very likely to repeat part of the sequence it just followed. We call this phenomenon “repeated motions”.

Another property contributes to the broken ergodicity is the symmetry between the forward iteration and the backward iteration. By comparing Eqs. (3) and (4), it is easy to see the forward and backward iterations are symmetric with respect to the line $\vartheta = a/2$, as illustrated in Fig. 2. In other words, if point (ϑ, x) corresponds to bi-infinite sequence $\cdots Q_3 Q_2 Q_1 \bullet P_1 P_2 P_3 \cdots$, its symmetric point $(a - \vartheta, x)$ corresponds to $\cdots P_3 P_2 P_1 \bullet Q_1 Q_2 Q_3 \cdots$. Actually, this symmetry is the time reversal symmetry in the original model, and two reflection symmetric points correspond to the same state of the particle but viewed in two opposite time directions.

This reflection symmetry generates “retraced motions” in symbolic sequences. An M iteration brings ϑ to $a - \vartheta$, which is equal to reflecting about line $\vartheta = a/2$. Consider an initial point $(a - \vartheta, 1 + a - \vartheta - x)$ which is in M region, i.e., it corresponds to a bi-infinite sequence $\cdots Q_2 Q_1 \bullet M P_1 P_2 \cdots$, then its symmetric point $(\vartheta, 1 + a - \vartheta - x)$ corresponds to $\cdots P_2 P_1 M \bullet Q_1 Q_2 \cdots$. Meanwhile, a forward iteration will map the point $(a - \vartheta, 1 + a - \vartheta - x)$ to (ϑ, x) and bring its sequence to $\cdots Q_2 Q_1 M \bullet P_1 P_2 \cdots$. Notice that the symmetric point $(\vartheta, 1 + a - \vartheta - x)$ and the image (ϑ, x) have equal ϑ value, their sequences tend to share a long common string. In general, the smaller the distance $|1 + a - \vartheta - 2x|$ is, the longer their common string is. Assume the first k letters in the two sequences are identical, then we have $P_i = Q_i$ for $i \leq k$. Look at this result in $\cdots Q_2 Q_1 M \bullet P_1 P_2 \cdots$, the sequence of (ϑ, x) , it means that when the trajectory meet the M , it retraces k iterations in the sequence, and bring the \tilde{n} of the sequence back to k iterations ago. We call this phenomenon “retraced motions”.

It is easy to see that both repeated motions and retraced motions generate many symbolic fragments whose $\tilde{n} = 0$, thus keep the \tilde{n} values the same with and without these symbolic fragments. In addition, these two kinds of motions work synergistically. A retraced motion is very likely to trigger a repeated motion, and a repeated motion replicates the retraced motions in its arrange. Besides, both kinds of motions occur in various time scales. Several short-time motions construct a long-time motion, then several such long-time motions construct an even longer-time one, etc. The time scale of the motions heavily depend on $|1 + a - \vartheta - 2x|$ or $|x - x'|$. As the number of iterations increases, there are

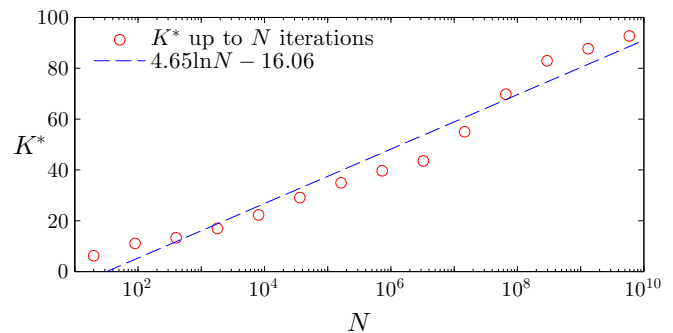


FIG. 5: The dependence of K^* on N . The control parameter is $a = 2 \sin(\frac{\sqrt{5}}{2}\pi)$, i.e. $\alpha = \frac{\sqrt{5}-1}{4}\pi$. An average ensemble of 500 trajectories is taken. All initial points of the trajectories have fixed initial $\vartheta_0 = \sqrt{2}$, with randomly chose initial $x_0 \in [0, 1]$. The dash line $\sim 4.65 \ln N - 16.06$ is plotted for reference.

more phase points whose coordinate values make one of the distances very tiny. As a result, longer and longer-time motions appear in the sequence, and the waiting time to take a new ϑ value increases fast.

VI. DISCUSSION

Let K^* be the number of different ϑ values a trajectory has taken up to N iterations. We evolve an ensemble of trajectories with the same initial ϑ_0 but with random initial x_0 in the interval $[0, 1]$ in order to explore the dependence of K^* on N . The result is shown in Fig. 5. The main outcome is that despite some fluctuations K^* increases about linearly with $\ln N$ as $N \leq 10^{10}$. This numerical evidence suggests that the iteration time N requested to take K^* different ϑ values increases exponentially with K^* , thus strongly confirms our conclusion that a trajectory will visit only a small fraction of the allowed ϑ values in any meaningful time scale.

Our proof is in nice agreement with previous numerical studies [11, 12]. In addition, the main result of Ref. [15], namely, the trajectory of almost every initial point with $\vartheta_0 \in \{\pm 1, a/2\}$ in an arbitrary right triangular billiard is periodic, can be viewed as a special case of our conclusion. However, as mentioned in Sec. I, there is a contradiction between previous studies that need to be explained. In Ref. [10], Vorobets proved that if the numbers α_i/π admit a certain super-exponentially fast rational approximation, where α_i are the vertex angles of the polygon, then the billiard flow has identical ergodic properties with that in the rational polygons. In particular, he suggested that with some kind of weak irrational α , the right triangular billiard flow is ergodic based on the ergodicity of rational polygonal billiards. But rational right triangular billiard flow is, unlike that in general polygons, not ergodic [8]. Therefore, his suggestion is incorrect, which explains the contradiction.

Our proof shows that irrational right triangular billiard is an explicit example of irrational but nonergodic polygonal billiards, thus provide an answer to an open question listed in Ref. [7]. In addition, though general polygonal billiards are believed to be ergodic, isosceles triangular and rhombic billiards, whose dynamics are exactly equivalent to that of right triangular billiard, are two additional examples.

Right triangular billiard system has been studied for

decades [15–18]. Previous studies explored the properties of the trajectories mainly using diagram methods, which might create confusion in some cases. On contrast, our method based on the piecewise map is much easier to manipulate and verify. For example, one can easily exam whether a special combination of collisions exists, or the exact angle of the particle after a big number of certain collisions. We think it will become a powerful tool for further related study.

-
- [1] D. L. Stein and C. M. Newman, *Phys. Rev. E* **51**, 5228 (1995).
 - [2] L.F. Cugliandolo and J. Kurchan, *Phil. Mag. B* **71**, 501–514 (1995).
 - [3] Y. Wang, X. Ren, K. Otsuka, and A. Saxena, *Phys. Rev. B* **76**, 132201 (2007).
 - [4] A. Rebenshtok and E. Barkai, *Phys. Rev. Lett.* **99**, 210601 (2007).
 - [5] E. Gutkin, *J. Stat. Phys.* **83**, 7–26 (1996).
 - [6] S. Kerckhoff, H. Masur, and J. Smillie, *Ann. Math.* **124**, 293–311 (1986).
 - [7] E. Gutkin, *Chaos* **22**, 6116 (2012).
 - [8] R. Artuso, G. Casati, and I. Guarneri, *Phys. Rev. E* **55**, 6384 (1997).
 - [9] I. P. Cornfeld, S. V. Fomin, and Y. G. Sinai, *Ergodic Theory* (Springer, Berlin, 2012).
 - [10] Y. B. Vorobets, *Sb. Math.* **188**, 389 (1997).
 - [11] M. Hasegawa, *Phys. Lett. A* **242**, 19–24 (1998).
 - [12] J. Wang, G. Casati, and T. Prosen, *Phys. Rev. E* **89**, 042918 (2014).
 - [13] A. J. Lichtenberg and M. A. Leiberman, *Regular and Stochastic Motion* (Springer, Berlin, 2013).
 - [14] B. Hao and W. Zheng, *Applied Symbolic Dynamics and Chaos*, (World Scientific, Singapore, 1998).
 - [15] B. Cipra, R. M. Hanson, and A. Kolan, *Phys. Rev. E* **52**, 2066 (1995).
 - [16] S. Troubetzkoy, *Ann. Inst. Fourier* **55**, 29–46 (2005).
 - [17] W. P. Hooper, *Geom. Dedic.* **125**, 39–46 (2007).
 - [18] G. Galperin and D. Zvonkine, *Regul. Chaotic Dyn.* **8**, 29–44 (2003).